Supporting Information

Highly efficient charge inversion in dense periodic nanoporous framework membranes

Yan Wang,[b,1] Shixian Xin,[b,1] Yunyang Wang,[c] Han Xie,[b] Fuhao Yao,[b] Linghao Liu,[b] Jinlei Yang,[b] and Yaping Feng*,[a]*

a. College of Materials Science and Engineering, Beijing University of Chemical Technology, Beijing 100029, P.R. China.
E-mail: ypfeng@buct.edu.cn
b. School of Nanoscience and Engineering, School of Chemical Sciences, University of Chinese Academy of Sciences, Beijing 100049, P.R. China.
E-mail: yangjinlei@ucas.ac.cn
c. National Center for Nanoscience and Technology, Beijing 100190, P.R. China.
E-mail: wangyy2023@nanoctr.cn

Experimental Section

Materials

2,4,6-triformylphloroglucinol (Tp) was purchased from Aladdin. 2,5-diaminobenzenesulfonic acid (Pa-SO_3H) was obtained from Macklin. KCl ($\geq$ 99.8%), NaCl ($\geq$ 99.8%), LiCl ($\geq$ 99.0%), $MgCl_2 \cdot 6H_2O$ ($\geq$ 99.0%), $CaCl_2$ ($\geq$ 96%) and $LaCl_3 \cdot 6H_2O$ ($\geq$ 99.99%) were purchased from Aladdin. PTFE microporous membranes were purchased from MREDA. All other reagents were obtained from Beijing Chemical Works.

Synthesis of the TpPa-SO_3H covalent organic framework (COF) membrane

First, a 3 mM aqueous solution of Pa-SO_3H containing 3 M acetic acid was poured into a funnel. A PTFE substrate was tilted at a 15° angle and immersed in the aqueous phase. Subsequently, a 2 mM toluene solution of Tp was slowly added to form a sharp and stable interface between the organic phase and the aqueous phase. After injection, the two monomers gradually polymerized at the interface over three days at room temperature, yielding a macroscopic orange-red membrane. After the reaction, slowly drained the solution was drained from the funnel, allowing the COF membrane to gradually deposit onto the substrate. The resulting membrane was dried at ambient temperature and carefully rinsed with methanol.

Calculation of Critical Inversion Concentration (crc)

Mean-field theory is commonly applied to describe the diffusion layer, while strongly correlated liquids (SCL) theory is employed to model ion-surface and ion-ion interactions within the Stern layer. The SCL theory provides a analytical prediction for the critical ion concentration at which charge inversion occurs[1-4]:

$$c_{crc} = |\frac{\sigma_b}{2r_{ion}Ze}| exp(\frac{\mu_c}{k_BT})$$

The electrochemical potentials of Z-valent ions in the bulk and the Stern layer are given by[2,5]:

$$\mu_b = \mu_b^0 + k_BTlnC_{b,0} + Ze\varphi_\infty$$

$$\mu_s = \mu_s^0 + k_BTln(\frac{n}{2r_{ion}}) + Ze\varphi_s$$

where $C_{b,0}$ is the bulk concentration of Z-ion. φ_∞ and φ_s are the electrochemical potentials of the bulk phase and the Stern layer, respectively. In a state of equilibrium, $\mu_b = \mu_s$ and $\varphi_\infty = 0$, yielding:

$$\mu_0 + k_BTlnC_{b,0} = k_BTln(\frac{n}{2r_{ion}}) + Ze\varphi_s$$

Among them, $\mu_0 = \mu_i + \mu_c$ includes all ion-surface interactions, where μ_i accounts for hydration and specific binding effects, and μ_c is the chemical potential arising from ion correlations, given by[1-3]:

$$\mu_c = -k_BT(1.65\Gamma - 2.61\Gamma^{\frac{1}{4}} + 0.26ln\Gamma + 1.95)$$

In SCL theory, ion correlation is considered the primary cause of charge inversion. The coupling parameter Γ is defined as:

$$\Gamma = \frac{1}{4k_BT\varepsilon_f}\sqrt{\frac{|e^3Z^3\sigma_b|}{\pi}}$$

Preparation of COF powder

Tp (169.4 mg) and Pa-SO_3H (126.0 mg) were weighed into a Pyrex tube. Add 3 mL of as A mixed solvent system of n-butanol (3 mL) and o-dichlorobenzene (3 mL) was added, followed by 1.2 mL of acetic acid aqueous solution (6 M) as the reaction catalyst.[6] After ultrasonic dispersion for 2 minutes, completely immerse the reaction system in

liquid nitrogen until fully solidified. The tube was evacuated and slowly warmed to room temperature to release dissolved gases. This freeze-thaw cycle was repeated three times. The sealed tube was heated in silicone oil at 120°C for 72 hours. After reaction, the product was collected by filtration, washed thoroughly with ethanol and tetrahydrofuran (THF), and finally dried under vacuum at 100°C for 12 hours to obtain a red powder.

Calculation of K^+ adsorption by COF

The K^+ adsorption capacity was calculated by the following equation[7]:

$$Capacity = \frac{(C_0 - C_e)V}{m}$$

To account for weakly adsorbed K^+, the TpPa-SO_3H powder was washed ten times with 10 mL of deionized water. The ion concentration in the combined filtrate was measured, and the amount of residual K^+ was subtracted to determine the net adsorption capacity, which was calculated to be 0.285 mmol g^{-1}. The BET surface area of TpPa-SO_3H is 113.27 m^2/g, with an average pore size of 1.27 nm. From this, the number of nanopores was estimated, indicating that each nanopore captured approximately 3.2 K^+ ions on average.

Table of Contents

Supplementary Figure S1:

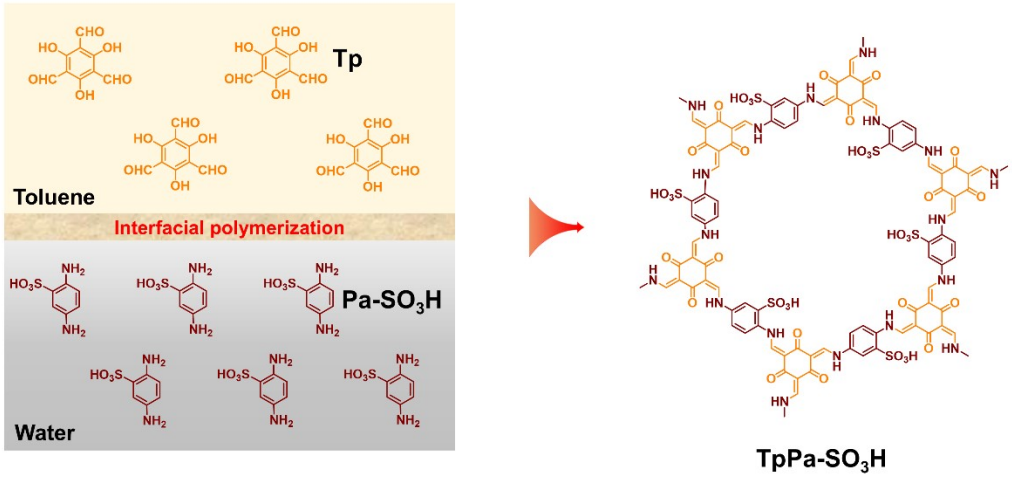

Figure S1. Synthesis process and molecular structure of the TpPa-SO_3H membrane.

Supplementary Figure S2:

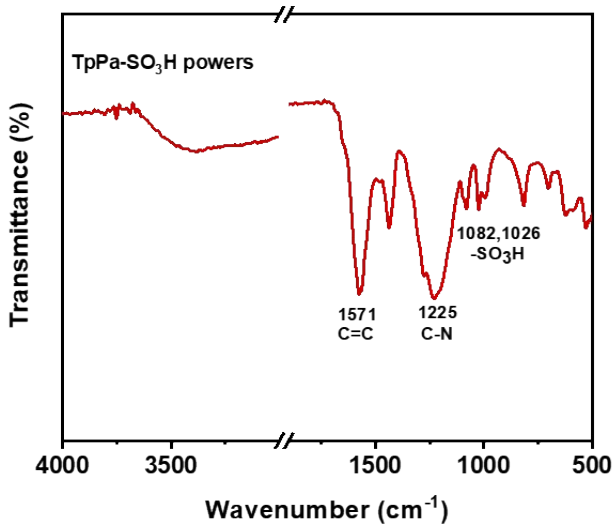

Figure S2. FTIR spectra of TpPa-SO_3H powders.

Supplementary Figure S3:

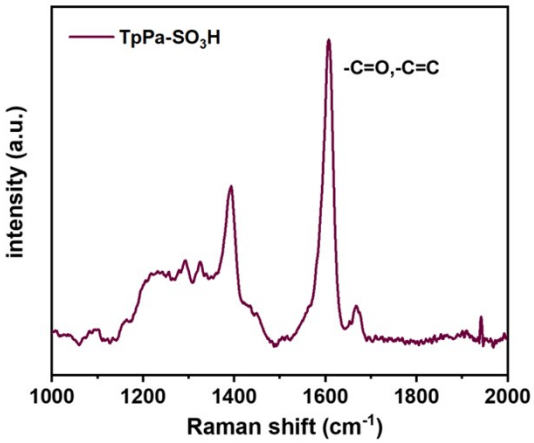

Figure S3. Raman spectrum of the TpPa-SO_3H membrane. The appearance of characteristic peaks at 1394, 1608, and 1666 cm^{-1} confirmed its successful formation.

Supplementary Figure S4:

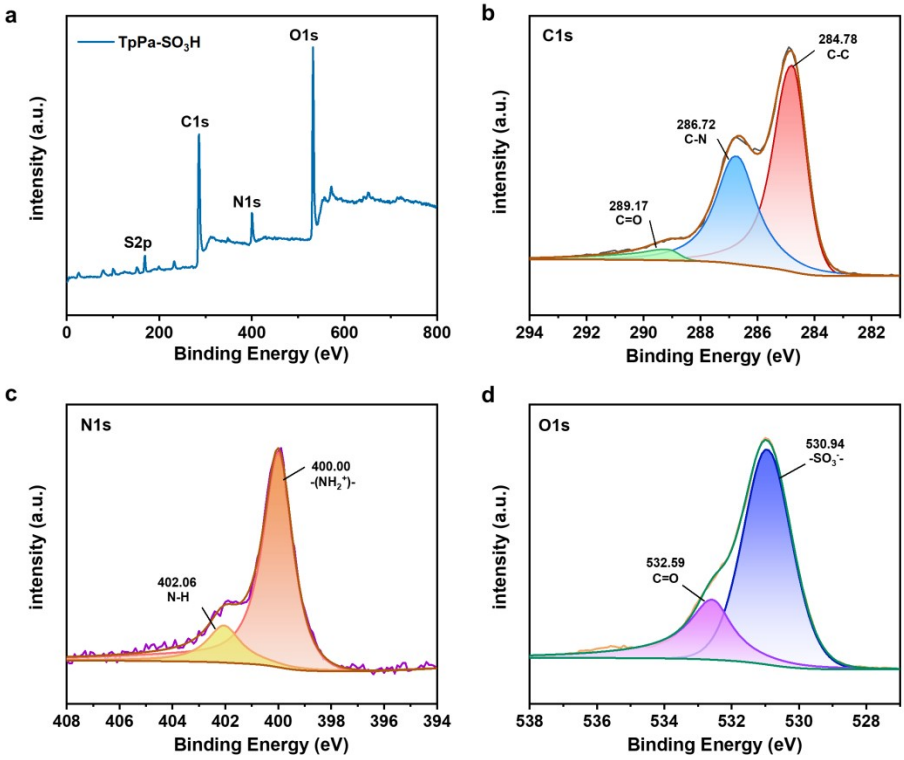

Figure S4. XPS spectra of TpPa-SO_3H membrane.

Supplementary Figure S5:

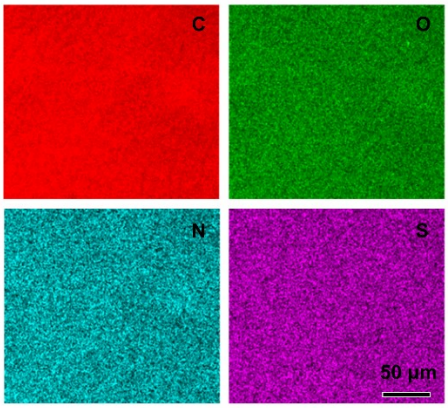

Figure S5. Elemental mapping of the TpPa-SO_3H membrane by SEM-EDS.

Supplementary Figure S6:

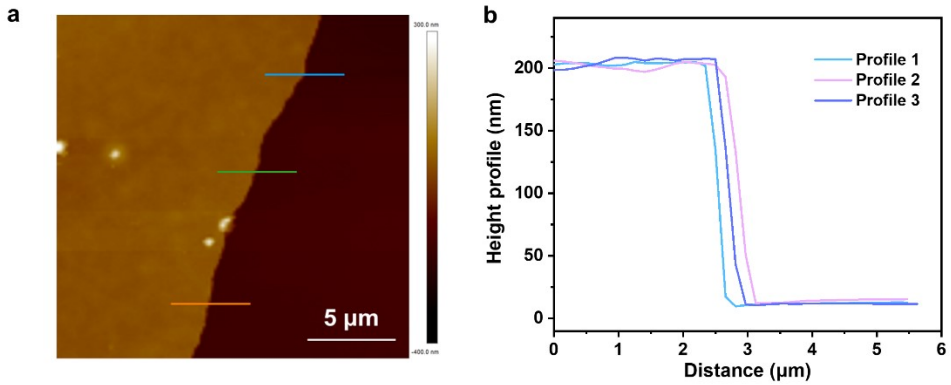

Figure S6. a) AFM height image of TpPa-SO_3H membrane. b) AFM height profile.

Supplementary Figure S7:

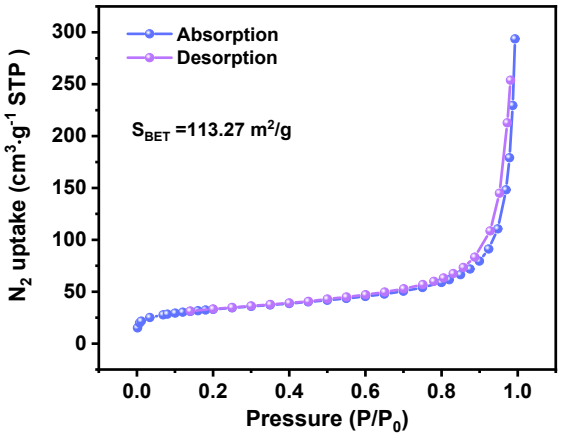

Figure S7. N_2 adsorption-desorption isotherms of TpPa-SO_3H COF.

Supplementary Figure S8:

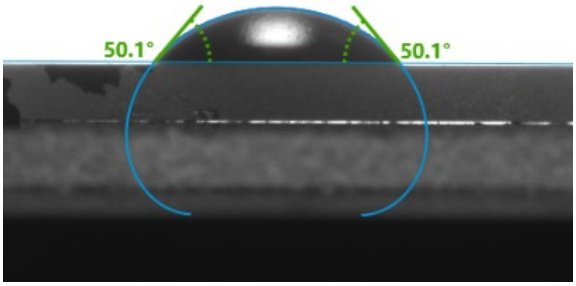

Figure S8. Water contact angle measurement of the TpPa-SO_3H membrane.

Supplementary Figure S9:

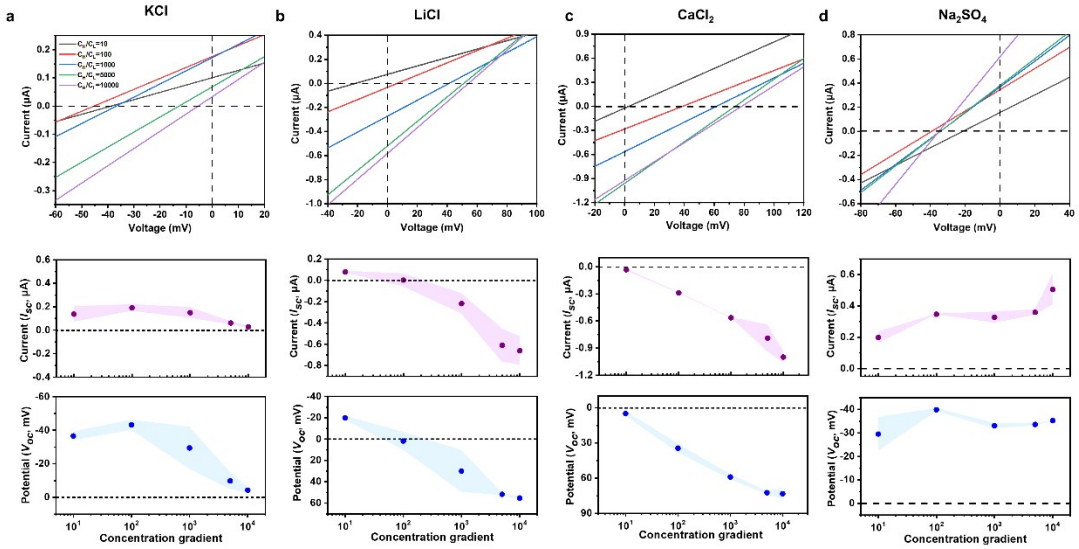

Figure S9. Ion selectivity of the TpPa-SO_3H membrane in different salt solutions. a-d) Current-voltage (I-V) curves (top) and corresponding short-circuit current, *Isc* (middle) and open-circuit voltage, *Voc* (bottom) as a function of concentration gradient measured in KCl, $LiCl_2$, $CaCl_2$ and Na_2SO_4 solutions, respectively. Error bars represent standard deviation (s.d.) with three independent measurements.

Supplementary Figure S10:

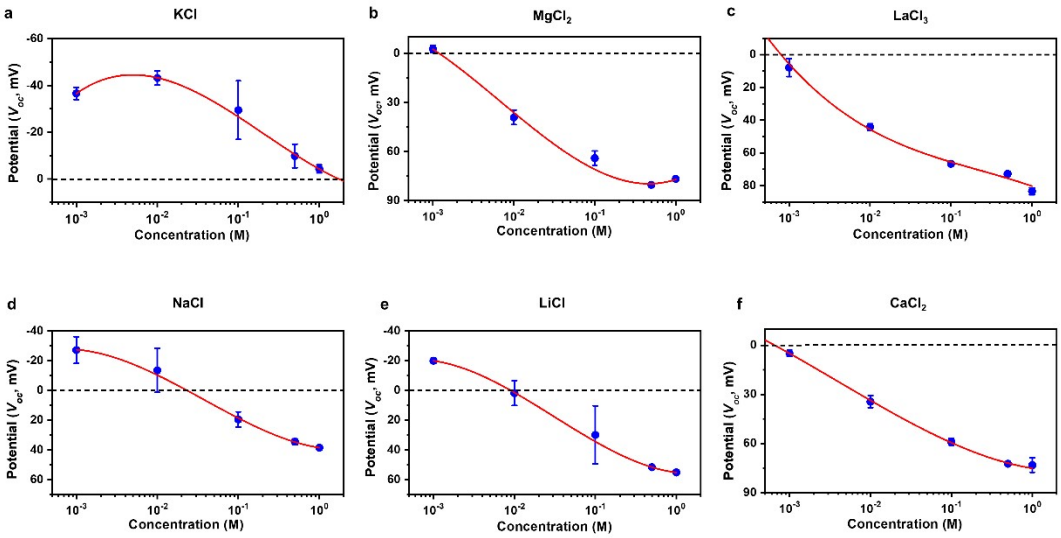

Figure S10. Fitted curves of V_{OC} and C_H for determining the critical reversal concentration (*crc*).

Supplementary Figure S11:

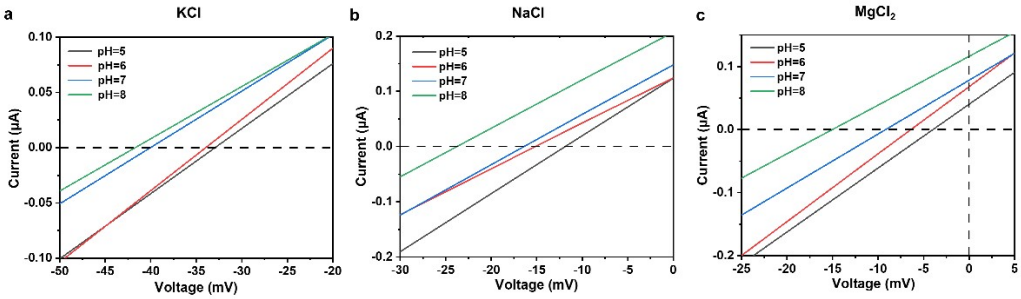

Figure S11. Reversal potential as a function of pH in KCl, NaCl, and $MgCl_2$ solutions under a fixed concentration gradient of 10. C_H = 10 mM, C_L = 1 mM.

Supplementary Figure S12:

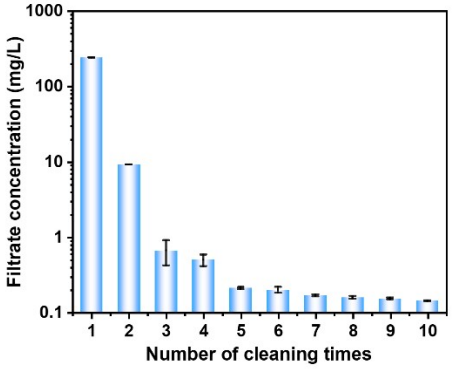

Figure S12. Decline of K^+ concentration in the filtrate during successive washing cycles. The substantial decrease in the first four washes confirmed that residual K^+ introduces significant error and must be excluded**.**

Table S1. Summary of the analyzed species and their corresponding bare radii, hydrated radii, and hydration energies.[8,9]

Ion type	bare radius (Å)	hydrated radius (Å)	hydration energy (KJ mol^{-1})
K^+	1.33	3.31	-295
Na^+	0.95	3.58	-365
Li^+	0.6	3.82	-475
Ca^{2+}	0.99	4.12	-1505
Mg^{2+}	0.65	4.27	-1830
La^{3+}	1.06	4.52	-3285
Cl^-	1.81	3.32	-384
SO_4^{2-}	2.9	3.79	—

References

1 F. H. J. v. d. Heyden, D. Stein, K. Besteman, S. G. Lemay and C. Dekker, *Phys. Rev. Lett.*, **2006,** 96.

2 K. Besteman, M. A. G. Zevenbergen and S. G. Lemay, *Phys. Rev. E*, **2005,** 72, 501.

3 K. Lin, C.-Y. Lin, J. W. Polster, Y. Chen and Z. S. Siwy, *J. Am. Chem. Soc.*, **2020,** 142, 2925-2934.

4 K. Besteman, M. A. G. Zevenbergen, H. A. Heering and S. G. Lemay, *Phys. Rev. Lett.*, **2004,** 93, 170802.

5 T. T. Nguyen, A. Y. Grosberg and B. I. Shklovskii, *J. Chem. Phys.*, **2000,** 113, 1110-1125.

6 K. Li, T.-X. Luan, Z. Wang, J.-R. Wang and P.-Z. Li, *ACS Appl. Nano Mater.*, **2022,** 5, 15228-15236.

7 G. Wang, L. Shao and S. Zhang, *Adv. Mater.*, **2025,** 37, 2414898.

8 C. P. Kelly, C. J. Cramer and D. G. Truhlar, *J. Phys. Chem. B*, **2006,** 32, 16066–16081.

9 Q. Wen, D. Yan, F. Liu, M. Wang, Y. Ling, P. Wang, P. Kluth, D. Schauries, C. Trautmann, P. Apel, W. Guo, G. Xiao, J. Liu, J. Xue and Y. Wang, *Adv. Funct. Mater.*, **2016,** 26, 5796-5803.